

EVALUATION OF BUILDING DEFORMATION MONITORING USING STEREOPHOTOGRAMMETRY METHOD AND KALMAN FILTER MODEL

AUTHORS:

A. S. Alademomi^{1,*}, O. A. Jimoh², E. E. Atojunere³, A. O. Alabi⁴, S. A. Ishola⁵, I. V. Ayantayo-Ojo⁶, T. J. Salami⁷, and J. O. Odumosu⁸

AFFILIATIONS:

^{1,2,4,5,6,7}Department of Surveying and Geoinformatics, Faculty of Engineering, University of Lagos, Nigeria.

¹Centre for Multidisciplinary Research and Innovation, Suite C59, New Bannex Plaza, Wuze 2, Abuja, Nigeria.

³Department of Soil Science and Biosystems Engineering, Fiji National University, Fiji Islands, Oceania.

⁸Department of Surveying and Geoinformatics, Federal University, Oye Ekiti, Nigeria.

*CORRESPONDING AUTHOR:

Email: salademomi@unilag.edu.ng

ARTICLE HISTORY:

Received: 25 January, 2024.

Revised: 03 April, 2024.

Accepted: 07 April, 2024.

Published: 12 June, 2024.

KEYWORDS:

Deformation monitoring, Building, Stereophotogrammetry, Kalman filter.

ARTICLE INCLUDES:

Peer review

DATA AVAILABILITY:

On request from author(s)

EDITORS:

Chidozie Charles Nnaji

FUNDING:

Lagos State Science Research and Innovation Council (LASRIC)

HOW TO CITE:

Alademomi, A. S., Jimoh, O. A., Atojunere, E. E., Alabi, A. O., Ishola, S. A., Ayantayo-Ojo, I. V., Salami, T. J., and Odumosu, J. O. "Evaluation of Building Deformation Monitoring using Stereophotogrammetry Method and Kalman Filter Model", *Nigerian Journal of Technology*, 2024; 43(2), pp. 232 – 239; <https://doi.org/10.4314/njt.v43i2.5>

Abstract

This research investigates building deformation monitoring using stereophotogrammetry and integrating the Kalman filter to refine the result with conventional geodetic measurements being the baseline. By refining stereophotogrammetric coordinates with the Kalman filter, the study aims to improve measurement precision in the detection of displacement which is a measure of differences in converted stereo-coordinates obtained from the observed points over time. The refined coordinates exhibited higher accuracy compared to raw stereophotogrammetric measurements, highlighting the effectiveness of the proposed approach in reducing observational errors and relatively detected and quantified building deformations with an average rate of displacement of 0.025978169 m/epoch in the x-axis, 0.030498323 m/epoch in the y-axis, and 0.014078842 m/epoch in the z-direction, and a range of 0.000155 m/epoch to 0.593497 m/epoch. Points P03 (0.008 m/epoch), PH04 (0.021 m/epoch), and PH22 (0.037 m/epoch) on the monitored building indicated the highest displacement. This research contributes to the field of knowledge in the area of deformation monitoring by offering an innovative methodology for accurate assessment of building deformation. In the overview, this research demonstrates the potential of a simple, efficient, and cost-effective method of monitoring deformation that can ensure the safety and sustainability of engineering structures.

1.0 INTRODUCTION

Deformation monitoring studies change due to applied stress on structures [1]. Deformation monitoring is essential for computation, analysis, and maintenance of observed changes in engineering structures over time due to environmental factors and aging, in the analysis of impacts on their shape, size, and strength [2 - 4]. In addition to jeopardizing public health and safety, environmental contamination and significant economic loss are also of major concern in the failure of structures [5 - 7]. In the past 50 years, building collapses in Lagos State, Nigeria have claimed over 400 lives. Report from a Government investigation indicated that between 2007 and 2013, there were at least 135 cases. A research done by Awoyera et. al in [8] outlined about 42 major cases of building collapse that occurred between 2010 – 2019 across various states in Nigeria with about 415 casualties.

Multi-storey buildings often account for the majority of failed structures [9, 10]. Worth mentioning here is that the rheological properties of the underlain soil (which deals with soil strength and the amount of

Vol. 43, No. 2, June 2024

water) can assist in studying the failure rate of structures [11]. The high recurrence of building failure in Lagos, Nigeria for example might not be unconnected to the constant threat of sea-water encroachment on land that weakened building foundations thereby causing structural instability [8]. The importance of building deformation monitoring to combat structural failure cannot be overemphasized [9, 10].

Structural deformation studies led to monitoring methods and BIM applications [12, 13]. Adapted methods from [8, 14 - 17] used photogrammetry for deformation measurement, despite camera and environmental limitations. Apart from procedural methods, the use of photogrammetric software and algorithms like Photo Modeler and Vision Metrology System (VMS) for building deformation analysis and comparison are being considered by other authors [2, 18 - 20]. The photogrammetric method for studying and predicting the deformation of buildings is considered to be fast, accurate, cost-effective, and reliable in studying the deformation of buildings [18]. Structural deformation tracking uses either geodetic surveys or geotechnical measurements depending on the monitoring objective, both allow for quality evaluation and error detection. Stereophotogrammetry, overcoming conventional methods' limitations, is viable for deformation analysis due to its accuracy and cost-effectiveness [2, 18, 21].

For deformation studies vital variables of measurement include; point positions, velocity, orientation, and network of control points [22]. Thus, observed quantities of interest are point coordinates (x, y, z) with respect to time t of observation. Quantities subjected for analysis would result in horizontal $(\Delta x, \Delta y)$ and vertical displacement (Δz) . These can be extracted from stereo-photogrammetry, while Kalman Filtering could further discover the appropriate time function description of point movements without taking into account any potential relationships to causal factors [23].

Mathematically, the Kalman filtering equations are expressed as follows;

$$X_k = \varphi_{k,k-1}X_{k-1} + W_k \quad (1)$$

$$I_k = (A_k X_k) + V_k \quad (2)$$

Where; X_k = state vector at time t_k ; X_{k-1} = state vector at time t_{k-1} ; $\varphi_{k,k-1}$ = transition matrix from time t_0 , to t_k ; W_k = noise vector representing the dynamic model at time t_k ; I_k = observation vector at time t_k ; A_k = design matrix for the measurement model; V_k = noise vector, which represents the measurement model at time t_k .



© 2024 by the author(s). Licensee NIJOTECH.

This article is open access under the CC BY-NC-ND license.

<http://creativecommons.org/licenses/by-nc-nd/4.0/>

The filter algorithm has been used extensively in building deformation studies where geodetic surveys are used for deformation monitoring [15, 23, 24]. This study evaluates the effectiveness of combining stereo photogrammetry with the Kalman filter algorithm for monitoring deformation in engineering structures with the aid of network of highly accurate ground controls points (GCPs) and precise measurement from points of interest (Photo control points, PCPs) on a building within a coastal zone with documented instances of deformation.

2.0 MATERIALS AND METHODS

Data used for this study span a period of 3 months with the subsequent sections undertaken.

2.1 Study Area

The target building was the National Centre for Energy Efficiency and Conservation (NCEEC) building at the University of Lagos. Located on Oduduwa Drive in Akoka, Lagos (see Figure 1), the recently inaugurated 16-meter tall structure has a history of deformations. While measures have been taken to address stability concerns, this research aims to monitor the building's ongoing structural health.

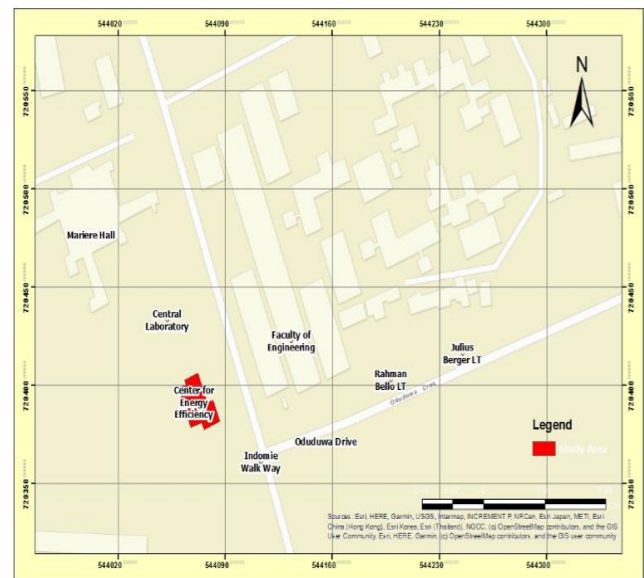


Figure 1: Study area

2.2 Data Collection

This section involves the data collection process and the methods deployed for the acquisition of the data.

2.2.1 Field and office reconnaissance

From field investigation and desk study, Table 1 shows the coordinates of the reference stations selected and used based on suggestions by [2]. Four (4) monitoring station points were established while ten (10) photo points were marked out during this

section based on the suggestion by [16]. Table 1, Figures 2 and 3 show the coordinates of the existing controls, GNSS setup on UL01 control, and the photo points marked out on the image respectively.

Table 1: Coordinates of existing controls

Control ID	X (m)	Y (m)	Z (m)
UL01	544473.954	720456.860	1.371
CREF0001	544172.860	720456.664	17.948



Figure 2: GNSS setup on UL01



Figure 3: Photo Control Points (PCP) on the image

2.2.2 Instruments used

The instruments used were:

- A Non-Metric Camera (Canon EOS 200D)
- M3 Trimble Total Station and accessories
- Trimble R8 GNSS and accessories

2.2.3 Control establishment and network adjustment

Using Static GNSS survey and post-processing techniques, the X,Y,Z point coordinates of the monitoring stations were determined. For the purpose of rigorous network adjustment and high reliability of the determined coordinates, a repeat observation was done using UL0.

Table 2: Coordinates of observed control stations

Control ID	X (m)	Y (m)	Z (m)
CREF0001	544172.860	720456.664	17.948
PT01	544075.911	720425.676	2.403



PT02	544099.914	720430.131	0.897
PT03	544108.153	720407.175	0.842
PT04	544111.848	720376.306	0.613
UL01	544473.954	720456.860	1.371

2.2.4 Stereo-photogrammetry

This process involves using close-range photogrammetry principles to determine the X, Y, and Z coordinates of each photo point on a monitored building using Canon EOS 200D. To ensure error-free images, a plumb bob was used, with the focal length of the camera fixed for all instance of image acquisition at every monitoring station (see Figures 4 and 5).



Figure 4: Camera setup on a monitoring point



Figure 5: Total station setup on a monitoring point

2.2.5 Conventional geodetic survey

A geodetic survey was conducted using an M3 total station, with control checks and redundant observations from all monitoring stations to photo points on the building.

2.5 Data Processing

Stereo photos, initially in RAW format, were converted to PNG using Adobe Photoshop, then MATLAB was used to extract pixel coordinates and convert them to image coordinates by multiplying with the pixel size, which was subsequently transformed to ground coordinates using a polynomial adjustment technique based on known control points

from a conventional geodetic method; while using the adapted method from [2]. The Kalman filter algorithm was then used to refined the data by computing the error variance covariance matrix, using the difference between adjusted geodetic and stereo-photogrammetric data input, and assuming several variables to be zero, including the predicted state noise matrix (ω_k), control variable matrix (μ_k), and measurement noise (Z_m), thereby predicting more accurate data and determining the rate of velocity over a specified period [2].

3.0 RESULTS AND DISCUSSIONS

3.1 Results

Figure 6 depicts graphs generated from the x , y , and z coordinates of all PCPs via conventional, stereo-photogrammetry, and Kalman filter data. These graphical representations highlight the lines of best fit

across the three datasets, in order to determine the slope (velocity) of displacement. While Table 3 and 4 show coordinates averages from each methods used.

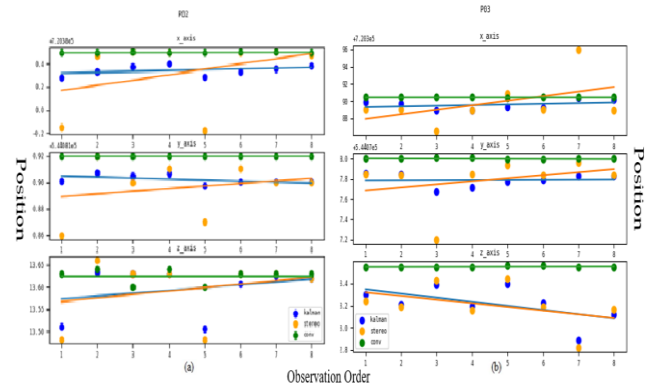


Figure 6: Graph of position versus observation order (time): (a) – for point P02; (b) – for point P03

Table 3: Coordinates averages by conventional and stereo-photogrammetry methods

PCP	Conventional			Stereo-photogrammetry		
	X	Y	Z	X	Y	Z
P03	720390.455	544078.000	13.553	720389.000	544077.800	13.170
P04	720404.775	544067.300	13.747	720405.800	544067.500	14.010
PH20.1	720389.554	544075.300	5.789	720392.000	544075.600	6.426
PH21.2	720403.24	544070.000	5.815	720401.300	544069.700	5.297
PH22.1	720404.579	544067.300	6.094	720406.200	544066.600	4.698
P02.1	720380.518	544081.900	13.638	720381.400	544084.300	12.870
P03.1	720390.649	544079.800	13.573	720390.700	544077.900	13.729
P04.1	720404.820	544067.500	13.779	720404.600	544067.500	13.579
PH01.1	720380.671	544081.800	3.094	720379.900	544081.100	3.003
PH02.1	720380.861	544081.600	6.163	720380.600	544081.900	5.911
PH03.1	720385.649	544079.800	7.431	720385.200	544079.200	7.477
PH04.1	720390.241	544078.000	7.469	720389.500	544076.100	7.864
PH20	720389.617	544075.300	5.807	720389.900	544075.100	6.068
PH21.1	720403.287	544070.000	5.909	720402.200	544066.300	6.909
PH22	720404.633	544067.300	6.123	720403.500	544065.400	7.078
P02	720380.505	544081.900	13.631	720380.500	544081.900	13.625
PH01	720380.641	544081.800	3.103	720380.600	544081.700	3.087
PH02	720380.826	544081.600	6.171	720380.800	544081.700	6.194
PH03	720385.611	544079.800	7.429	720385.600	544079.800	7.428
PH04	720390.203	544078.000	7.472	720389.400	544078.200	7.413

Table 4: Coordinates averages by Kalman filter and stereo-photogrammetry method

PCP	Stereo-photogrammetry			Kalman Filter		
	X	Y	Z	X	Y	Z
P03	720389.000	544077.800	13.170	720390.200	544077.800	13.122
P04	720405.800	544067.500	14.010	720405.100	544067.500	14.043
PH20.1	720392.000	544075.600	6.426	720400.600	544072.700	6.318
PH21.2	720401.300	544069.700	5.297	720405.000	544070.200	5.229
PH22.1	720406.200	544066.600	4.698	720407.700	544067.000	4.668
P02.1	720381.400	544084.300	12.870	720380.700	544082.600	13.022
P03.1	720390.700	544077.900	13.729	720390.400	544077.400	13.831
P04.1	720404.600	544067.500	13.579	720405.000	544068.300	13.572
PH01.1	720379.900	544081.100	3.003	720380.400	544081.500	2.968
PH02.1	720380.600	544081.900	5.911	720380.800	544081.700	5.930
PH03.1	720385.200	544079.200	7.477	720385.300	544079.200	7.486
PH04.1	720389.500	544076.100	7.864	720389.800	544076.700	7.852
PH20	720389.900	544075.100	6.068	720390.300	544075.900	6.012
PH21.1	720402.200	544066.300	6.909	720403.500	544069.600	6.773
PH22	720403.500	544065.400	7.078	720404.800	544068.400	6.909
P02	720380.500	544081.900	13.625	720380.400	544081.900	13.621
PH01	720380.600	544081.700	3.087	720380.600	544081.700	3.080
PH02	720380.800	544081.700	6.194	720380.800	544081.700	6.190
PH03	720385.600	544079.800	7.428	720385.700	544079.800	7.422
PH04	720389.400	544078.200	7.413	720388.600	544078.700	7.334



Figure 6a shows that point P02 has a moderate rate of displacement and a positive linear relationship among the three datasets. There is a contrast in the z-axis of P03 in Figure 6b which has a negative linear relationship among the datasets.

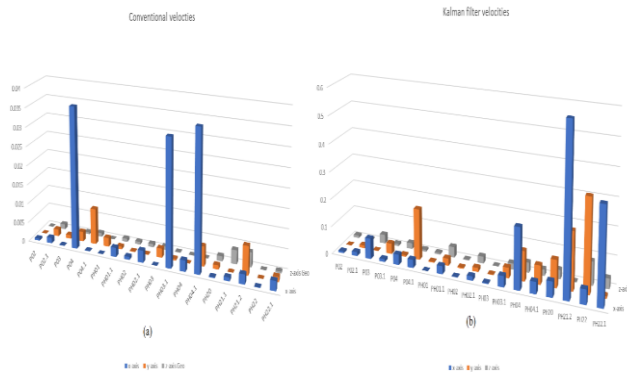


Figure 7: Graph of velocities obtained from: (a) – the conventional geodetic data, (b) – Kalman filter data

3.2 Discussions

3.2.1 Velocity of displacement/deformation

The conventional method yielded displacements per epoch (velocity) ranging from 8.81E-11m/epoch to 0.086107m/epoch with an average of 0.002115915 m/epoch in the x-direction, 0.0052901 m/epoch in the y-direction and 0.001234336m/epoch in the z-direction as shown in Figure 7a.

The results obtained from Stereo-photogrammetry revealed the highest velocity of displacement among the methods evaluated. The calculated velocities ranged from 0.000833 m/epoch to 0.705952 m/epoch. Such a range indicates an exceptionally high velocity of displacement. These unusually high values warrant further investigation. The velocities derived from the Kalman filter range from 0.000155m/epoch to 0.593497m/epoch with an average of 0.025978169 m/epoch in the x-axis, 0.030498323 m/epoch in the y-axis and 0.014078842 m/epoch in the z-direction as shown in Figure 7b.

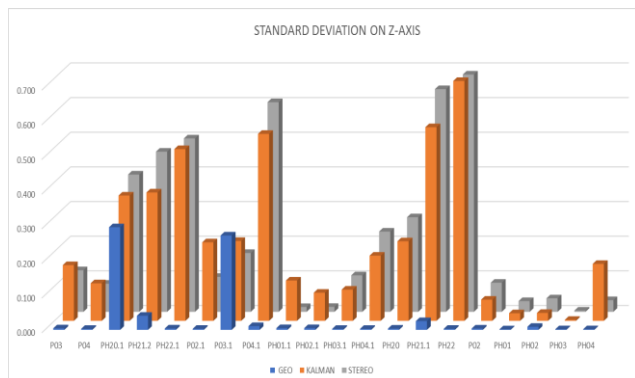


Figure 8: Z coordinates standard deviation

Figure 8 shows relationship among the computed Z coordinates via Geodetic survey, Stereo-Photogrammetry and KF techniques using a measure of the standard deviation. The strong relationship between the KF and stereo-photogrammetry techniques highlights the data linkage.

3.2.2 Horizontal accuracy

The KF exhibits higher accuracy along x and y axes (Figure 9 (a) and (b)). This discrepancy in accuracy may not necessarily be attributed to the workings of the algorithm itself but rather could be influenced by the characteristics of the stereo-photogrammetric data. It is possible that the measurements obtained through stereo-photogrammetry offer improved accuracy specifically along the x and y axes, or that the polynomial transformation employed enhances the horizontal precision.

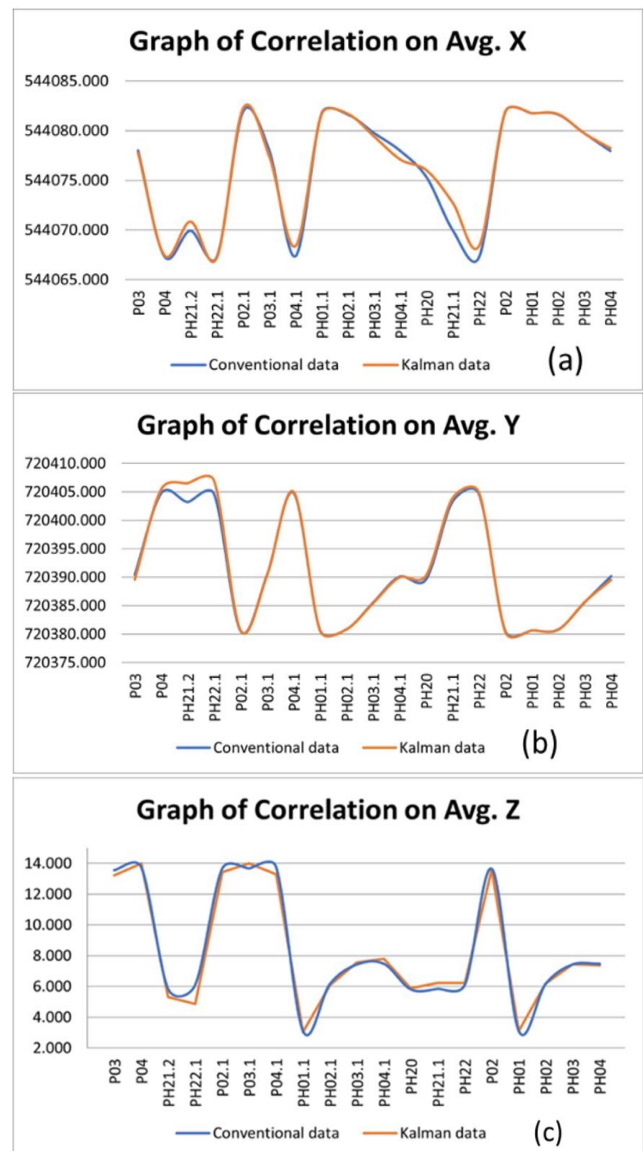


Figure. 9: Graph of correlation: (a) – x coordinates, (b) – y coordinates, and (c) – z coordinates

3.2.3 Vertical accuracy

The correlation graphs reveal that the Kalman Filter exhibits lower accuracy along the z axis (Figure 9(c)). This discrepancy in accuracy may not necessarily be attributed to the workings of the algorithm itself but rather could be influenced by the characteristics of the stereo data. It is possible that the measurements obtained through stereo-photogrammetry offer less accuracy specifically along the z axis, or that the polynomial transformation employed enhances the horizontal precision.

3.2.4 The conventional geodetic method

Based on the observations, the data and coordinates obtained through the conventional geodetic method, specifically using the total station, exhibited higher accuracy and provided more realistic values for the observations. As a result, the data acquired through this method was utilized as the baseline for comparing the results of the stereo-photogrammetric process with other techniques.

3.2.5 Statistical test on Z-values

An ANOVA analysis was conducted on both the individual z -values for each point and the average z -values per point. In the case of the individual z -values, the obtained p -value (0.139168) exceeds the significance level $\alpha = 0.05$, and the overall F value (1.981359) falls the critical F value (3.017202). Likewise, for the average z -values per point, the p -value (0.7326) surpasses $\alpha = 0.05$, and the overall F value (0.313717) is less than the critical F value (3.244818). Therefore, in both scenarios, the analysis results indicate that not all of the means within the three datasets are equal.

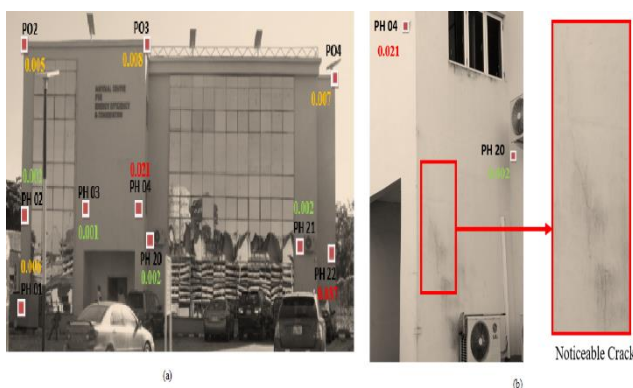


Figure 10: (a) Varying velocities in the vertical direction; (b) Noticeable vertical cracks close to PH04

3.2.6 Varying velocities in the vertical direction

Based on the analysis results, we observed varying velocities in the vertical direction at different photo points. These velocities were categorized as low, moderate, and high, represented by the colors green,



© 2024 by the author(s). Licensee NIJOTECH.

This article is open access under the CC BY-NC-ND license.

<http://creativecommons.org/licenses/by-nc-nd/4.0/>

orange, and red, respectively, in Figure 10a. The presence of high velocities indicates significant movement in the vicinity of these points, while low velocities indicate negligible displacements. A high velocity was observed along the column where PH04 was positioned (Figure 10b), which corresponds to the vertical cracks observed along that column. This high velocity may be attributed to tension or strain resulting from the load on the column or other contributing factors which could be subject to further investigation using the method posited by [25].

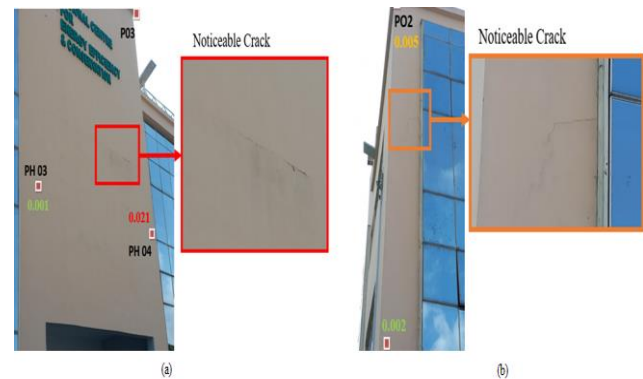


Figure 11: (a) Lateral crack identified on the beam above PH04, (b) Noticeable crack close to P02

Furthermore, a visible lateral crack was identified on the beam above PH04 (Figure 11a). The high velocity observed at PH04 provides additional insight into the situation. It appears to be a pressure point bearing a substantial weight, suggesting the possibility of significant displacement in that area. Additionally, near P02, a noticeable crack was detected (Figure 11b), coinciding with a moderately high velocity. This indicates tension in the column and suggests the presence of significant displacement in that particular region, potentially caused by similar factors as previously mentioned.

4.0 CONCLUSION

In this research, we employed the stereo-photogrammetry observation technique along with the Kalman Filter algorithm to collect and analyze the general possible displacements on the National Center for Energy Efficiency and Conservation (NCEEC) at The University of Lagos in Nigeria. By comparing the displacements predicted by the Kalman Filter algorithm and the conventional method, the study demonstrate the effectiveness of both the Kalman Filter algorithm and the stereo-photogrammetry observation technique. The Kalman Filter algorithm exhibited improved results compared to the stereo-photogrammetry method. When combined with proper calibration and knowledge of equipment specifications, the stereo-photogrammetry method

Vol. 43, No. 2, June 2024

<https://doi.org/10.4314/njt.v43i2.5>

proves to be a viable option for monitoring building deformations. This approach is particularly valuable as it reduces monitoring costs, simplifies the process, and saves time. Additionally, it enables the prediction of potential future deformations. The accessibility and affordability of high-capability digital cameras make the stereo-photogrammetry technique a practical choice for deformation monitoring, reducing the risks associated with preventable building collapses or structural failures. By gaining a better understanding of measurement and process noises, more precise models of everyday engineering structures can be easily analyzed using the stereo-photogrammetry method and the Kalman filter algorithm.

In this study, it was important to use the conventional method as a comparison and baseline since it was the first application with several unknown variables. This comparison allowed us to validate the effectiveness of the stereo-photogrammetry method and the Kalman Filter algorithm in this particular context.

5.0 ACKNOWLEDGMENTS

The authors would like to acknowledge the Lagos State Research Council for providing the grant used for the execution of the research, the Department of Surveying and Geoinformatics for providing a conducive environment, and some of the equipment that was used for the research. Lastly, we equally appreciate the Geospatial and Environmental Research Group for their intellectual contribution to the success of the work.

6.0 CONFLICTS OF INTEREST

The authors declare no conflict of interest.

REFERENCES

- [1] Mukupa, W. et al. "A review of the use of terrestrial laser scanning application for change detection and deformation monitoring of structures", *Survey Review*, 49; 2016: 116 - 99.
- [2] Odumosu, J., Adeleke, O., Chukwuemeka, V., Avoseh, O., and Ogundeji, O. "Stereophotogrammetry for 2-D building deformation monitoring using Kalman Filter. Reports on Geodesy and Geoinformatics", 110. 1-7. 10.2478/rgg-2020-0006. (2020).
- [3] Javanpour, M., and Zarfam, P. "Application of incremental dynamic analysis (IDA) method for studying the dynamic behavior of structures during earthquakes", *Engineering, Technology and Applied Science Research*, 2017, 7(1), 1338-1344.
- [4] Dammalage, T. L., and Jayasinghe, N. T. "Land-Use Change and Its Impact on Urban Flooding: A Case Study on Colombo District Flood on May 2016", *Engineering, Technology and Applied Science Research*, 9(2); 2019.
- [5] Gairns, C. "Development of Semi-Automated System for Structural Deformation Monitoring Using a Reflectorless Total Station", *M.Sc. Thesis, Department of Geodesy and Geomatics Engineering*, University of New Brunswick, Fredericton, Canada, 2008.
- [6] Alemdar, Z. F., Browning, J., and Olafsen, J. "Photogrammetric measurements of RC bridge column deformations", *Engineering structures*, 33(8):2407–2415; 2011.
- [7] Mokroš, M., Liang, X., Surový, P., Valent, P., Čerňava, J., Chudý, F., Tunák, D., Saloň, Š., and Merganič, J. "Evaluation of close-range photogrammetry image collection methods for estimating tree diameters", *ISPRS International Journal of Geo-Information*, 7(3), 2018.
- [8] Lee, H., and Han, D. "Deformation measurement of a railroad bridge using a photogrammetric board without control point survey", *Journal of Sensors*, 2018: 1–10,doi:10.1155/2018/6851252.
- [9] Olasunkanmi, H. O., and Abdullateef, I. B. "Exploring residential characteristics as determinants of household adaptation to climate change in Lagos, Nigeria", *International Journal of Disaster Resilience in the Built Environment*, 10.1108/IJDRBE-06-2021-0060, 2021.
- [10] Olagunju, R., Aremu, S., and Ogundele, J. "Incessant collapse of buildings in Nigeria: an architect's view", *Civil and Environmental Research*, 3(4):49–54; 2013.
- [11] Atojunere, E. E., Ogedengbe, K., and Afolayan, S. O. "Significance of Soil Rheological Properties to Tillage in Ilorin, North Central, Nigeria", *Institute of Science and Technology, Global Jour. of Eng. and Tech.*, (3)2: 253-256; 2010.
- [12] Jun, H., Ensheng, L., and Jiayu, Y. "Application of Structural Deformation Monitoring Based on Close-Range Photogrammetry Technology", *Advances in Civil Engineering*, Vol. 2021:1-11. DOI: 10.1155/2021/6621440, 2021.
- [13] Bhatti, I. A., Abdullah, A. H., Nagapan, S., Bhatti, N. B., Sohu, S., and Jhatial, A. A. "Implementation of building information modeling (BIM) in Pakistan construction industry", *Engineering, Technology and Applied Science Research*, 8(4), 3199-3202, 2018.



- [14] Odumosu, J. and Ajayi, O. “Comparative Analysis of some 2-D Transformation Models for Third Order Planimetric Mapping”, *International Journal of Advanced Scientific and Technical Research*, 2(4):385–404, 2014.
- [15] Chounta and Ioannidis “High Accuracy Deformation Monitoring of a Concrete Beam using Automatic Photogrammetric Techniques”, *International Federation of surveyors*, 2012.
- [16] Handayani, H. H., Yuwono, and Taufik, M. “Preliminary study of bridge deformation monitoring using GPS and CRP (case study: Suramadu Bridge)”, *Procedia Environmental Sciences*, vol. 24, pp. 266–276, 2015.
- [17] R  ther, H., Smit, J., and Kamamba, D. A. “Comparison of close-range photogrammetry to terrestrial laser scanning for heritage documentation”, *South African Journal of Geomatics*, 1(2):149–162, 2012.
- [18] Wang, C.-H., Mills, J. P., Gosling, P. D., Bridgens, B., and Gridale, R. J. “Monitoring the testing, construction and as-built condition of membrane structures by close range photogrammetry”, *In Proceedings of the ISPRS Commission V Mid-Term Symposium ‘Close Range Image Measurement Techniques’*, volume XXXVIII, pages 592–596, 21–24 June 2010, Newcastle upon Tyne, United Kingdom, 2010.
- [19] Fawzy, H. E.-D. “The Efficiency of Close-Range Photo-grammetry Instead of Precise Terrestrial Surveying Technique for Deformation Monitoring in Unstable Buildings”, *International Journal of Civil Engineering and Technology (IJCIET)*, 6(10):176–186, 2015.
- [20] Barazzetti, L., and Scaioni, M. “Development and implementation of image-based algorithms for measurement of deformations in material testing”, *Sensors*, vol. 10, no. 8, pp. 7469–7495, 2010.
- [21] Mills, J., and Barber, D. “Geomatics techniques for structural surveying”, *Journal of Surveying Engineering*, 130(2): 56 – 64, doi:10.1061/(ASCE)0733-9453(2004)130:2(56), 2004.
- [22] Alademomi, A. S., Mayaki, A. O., Daramola, O. E., Salami, T. J., and Olaleye, J. B. “Establishment of Deformation and Subsidence Monitoring Baseline in the Coastal Environment: A Case Study of University of Lagos”, *South African Journal of Geomatics*, DOI:10.4314/sajg.v9i1.2., 2020.
- [23] Ehigiator-Irughe, R., and Ehigiator, M. “Utilization of Kalman Filter Technique in Deformation Prediction of Above Surface Storage Tank”, *Journal of Advances in Physics Theories and Applications*, 21:18-23, 2013.
- [24] Gulal, E. “Structural deformations analysis by means of Kalman-filtering”, *Network of Scientific Journals from Latin America, the Caribbean, Spain and Portugal*, 19. 98-113. 10.1590/S1982-21702013000100007., 2013.
- [25] Benarbia, D., Benguediab, M., and Benguediab, S. “Two-dimensional analysis of cracks propagation in structures of concrete”, *Engineering, Technology and Applied Science Research*, 3(3), 429-432, 2013.

